CrystEngComm

Accepted Manuscript

ROYAL SOCIETY OF CHEMISTRY

www.rsc.org/crystengcomm

Cite this: DOI: 10.1039/c0xx00000x

www.rsc.org/xxxxxx

ARTICLE TYPE

Phase-Selective Hydrothermal Synthesis of Cu_2ZnSnS_4 Nanocrystals: The Effect of Sulphur Precursor

Vincent Tiing Tiong,[a] Yi Zhang[b], John Bell,[a] Hongxia Wang*[a]

Received (in XXX, XXX) Xth XXXXXXXXX 20XX, Accepted Xth XXXXXXXXX 20XX

DOI: 10.1039/b000000x

High quality Cu_2ZnSnS_4 (CZTS) films with uniform thickness and smooth surface were prepared using nanocrystals synthesized by a one-step hydrothermal method. It is found that the nature of sulphur precursor used in the hydrothermal reaction influence both the compositional purity and the crystal structure of the synthesized hydrothermal product significantly. CZTS material consisting of both wurtzite and kesterite crystal structures was obtained when using organic sulfur precursor such as thioacetamide and thiourea in the precursor solution of the hydrothermal reaction while pure kesterite phase CZTS nanocrystals were made when Na_2S was employed as the sulphur precursor. CZTS thin films deposited on a Mo-soda lime glass substrate with uniform thickness (1.7 μm) were made by a simple doctor-blading method. The investigation of the effect of thermal treatment on the film has indicated that wurtzite CZTS material was completely transformed to kesterite phase when the material was annealed at 550 ^oC. Large grains (around 2 μm in size) were found on the surface of the CZTS film which was annealed at 600 ^oC. The evaluation of photoresponse of the CZTS thin films has showed that a higher and very stable photocurrent was generated by the film annealed at 600 ^oC compared to the film annealed at 550 ^oC.

Introduction

High performance light absorbing materials for photovoltaic device that use earth abundant, non-toxic elements are highly desired to meet the global demand for large scale deployment of solar electricity with low environmental impact. The traditional light absorbing materials for PV such as $Cu(In_xGa_{1-x})S(Se)_2$ (CIGS) and CdTe uses scarce thus more expensive elements such as In, Ga, Te or toxic material like Cd.[1, 2] The world trading price of In and Ga is around $700/Kg and $1700/Kg at their peak demand, which impose a serious concern on the production scale of PV technologies using these materials. Hence, it is highly important to develop new alternative light absorbers that bear the merit of low material cost and low environment impact to tackle the global energy crisis. Among the various materials that have been developed, chalcopyrite-based light absorber material based on Cu_2ZnSnS_4 (CZTS) has shown promise for cost-effective solar cells. Compared to CIGS and CdTe, all the constituent elements in CZTS are richer in earth-crust, thus much cheaper and are environmentally benign. The abundance of zinc (Zn) and tin (Sn) in earth crust is 1500 times and 45 times greater than that of indium (In) and gallium (Ga) respectively.[3] Fundamentally, CZTS is an ideal light absorber for PV applications as well. Pure kesterite CZTS has a direct band gap of 1.5 eV and has a strong light absorption ability (light absorption coefficient $>10^4$ cm^{-1}) in the wavelength range from visible to near infrared of solar spectrum. According to Shockley-Queisser photon balanced calculations, the theoretical energy conversion efficiency of PV using light absorber material like CZTS is 31-33%.[4] Practically, a kesterite CZTS-based thin film solar cell with an energy conversion efficiency of 8.4% was reported, and this performance was further improved to 11.1% through selenization of CZTS (CZTSSe) absorber layer.[5, 6]

It is well-known that the crystal structure of light absorbing material determines its optoelectronic properties which in turn affect its performance in PV device. Traditionally, it is assumed that CZTS compound has two types of crystal structures: kesterite and stannite, and kesterite is the stable phase. The difference between them lies in the different arrangement of Cu^+ and Zn^{2+} in the crystal structure.[7] Nevertheless, recently, both theoretical calculation and experimental results have indicated that a third phase, wurtzite CZTS, may exist in this quaternary system at well.[7] DFT based theoretical calculation has indicated that the total energy of wurtzite-structured CZTS is much higher than that of kesterite and stannite.[8] The formation of wurtzite structure CZTS is not favourable thermodynamically, which is responsible for the rare observation of this crystal phase experimentally.

So far, all the reported wurtzite CZTS materials have been synthesized either by organic solvents based hot-inject method or solvothermal method, both of which use high boiling point organic solvent or solvent mixture in the reaction system, the experimental condition of which is less favourable in terms of environmental impact.[9-12] In this work, we employed a hydrothermal method which used water as the sole solvent for synthesis of CZTS quaternary compound. It has been found that

the nature of sulphur precursor in the hydrothermal reaction determines the formation and phase purity of the synthesized CZTS material. CZTS with pure kesterite phase was formed when inorganic sulphide Na_2S was used as the sulphur source while CZTS containing crystal structures of both kesterite and wurtzite was obtained when using an organic thioacetamide (TAA) as sulphur precursor. In contrast, the hydrothermal system using thiourea as sulphur source resulted in an impurity Cu_7S_4 together with CZTS with mixture wurtzite and kesterite crystal structure in the final product. The photoactivity of the synthesized CZTS nanocrystals was evaluated by fabrication of corresponding CZTS thin films with uniform thickness and smooth surface deposited on a Mo coated soda lime glass substrate (CZTS/Mo). The investigation on the influence of thermal treatment on the morphology and on the photoresponse of the CZTS thin films has shown that large grains were formed in the film at 600^{o}C, which led to the observation of a very stable photocurrent of the film under illumination.

Experiments

Preparation of materials

All the chemicals used in this work were provided by Sigma Aldrich and used as received unless otherwise stated. In a typical experimental procedure, analytical grade of copper (II) chloride dehydrate ($CuCl_2.2H_2O$, 0.2 mmol), zinc chloride ($ZnCl_2$, 0.1 mmol) product of BDH, tin (IV) chloride pentahydrate ($SnCl_4.5H_2O$, 0.1 mmol), sodium sulphide nonahydrate ($Na_2S.9H_2O$, 0.5 mmol) thioglycolic acid (TGA, 18 μL) were dissolved in 34 mL Mili-Q water under vigorous magnetic stirring. The solution was then transferred to a Teflon-lined stainless steel autoclave (Parr Instrument Company) of 45 mL capacity which was then sealed and maintained at 240°C for 24 h. After that, the autoclave was allowed to cool to room temperature naturally. The black precipitate was collected by centrifugation and washed with deionised water and absolute ethanol for several times to remove the ions in the end product. Finally, the product was vacuum-dried at 60°C for 5 h before further characterization. Similarly, the hydrothermal reaction which used thioacetamide (C_2H_5NS, TAA) or thiourea (CH_4N_2S, Tu) instead of Na_2S as sulphur source was undertaken under the same experimental conditions.

For simplicity, the CZTS material made from Na_2S sulphur precursor is named as: CZTS_Na_2S, and the material made from TAA based hydrothermal system is named as CZTS_TAA while the thiourea (Tu) based hydrothermal reaction is named as CZTS_Tu.

Deposition of CZTS thin films

A slurry containing the as-synthesized CZTS nanocrystals was prepared by dispersing CZTS material (10%, w/w) in mixture of terpineol and triton X-100 (85%:5%, w/w). The slurry was subject to rigorous magnetic stirring for 48 hours. Thin films were made by depositing the CZTS slurry on a molybdenum (Mo) coated soda lime glass (Mo/SLG) substrate by doctor-blading. The substrate was prewashed thoroughly with deionised water, acetone, and ethanol in sequence under sonication for 10 min followed by blow-dried with nitrogen gas. The thin film was then placed in a graphite box containing sulphur powder and annealed at 550°C or 600 ^{o}C for 30 min in a rapid thermal annealing processing (RTP) system with a heating rate of 10 °C/min. A static annealing atmosphere of 0.3 atm argon was supplied in the RTP furnace.

Characterisation

The crystallographic structure of the synthesized samples was identified by a multi-purpose X-ray diffractometer (XRD, PANanalytical XPert Pro, Cu Kα, λ = 0.154056 nm). A Raman spectrometer (Renishaw inVia Raman microscope) with the laser excitation wavelength of 532 nm was used to record Raman spectra of the materials at room temperature. The Raman spectra were collected by taking the average of 10 different spots. The morphology and composition of the samples were characterized by a field emission scanning electron microscope (FESEM, JEOL 7001F) at an acceleration voltage of 10.0 kV combined with an energy dispersive X-ray spectroscopy (EDS). Transmission electron microscopy (TEM) of the samples was performed on a JEOL JEM-1400 TEM microscope. High-resolution TEM (HRTEM) and selected area electron diffraction (SAED) images were obtained using JEOL JEM-2100 microscope at an accelerating voltage of 200 kV. Ultraviolet-visible (UV-vis) absorption spectrum of the CZTS nanomaterial which was dispersed in ethanol was measured using a Varian Cary 50 spectrometer. X-ray photoelectron spectrometer (XPS, Kratos Axis ULTRA) was employed to determine the valence state of each element of the samples. The photoresponse of the CZTS thin films were evaluated by a three-electrode photoelectrochemical (PEC) cell which consisted of CZTS/Mo/SLG based working electrode, platinum wire as counter electrode and Ag|AgCl reference electrodes in an aqueous electrolyte solution containing 0.2 M $Eu(NO_3)_3$ (pH = 2.3). The CZTS electrode was illuminated by a light emitting diode (LED, 532 nm) with light intensity of 50 mW/cm^2 under a constant potential of -300 mV (*vs* saturated Ag/AgCl reference electrode) The photocurrent generated by the PEC cell was recorded by an electrochemical workstation (VSP BioLogic Science Instruments).

Results and discussion

Influence of different sulphur source

The XRD patterns of the hydrothermal products which were synthesised using different sulphur sources are shown in Fig. 1(a). For ease of comparison, the standard XRD patterns of kesterite CZTS (JCPDS 01-75-4122) and simulated XRD pattern of wurtzite CZTS (see the Supporting Information for details) are also shown at the bottom in Fig. 1(a). It is found that all the four main peaks corresponding to the crystallographic planes of kesterite CZTS ((112), (220), (312) and (200)) can be found in all the hydrothermal products using different sulphur precursor. However, along with the peaks of kesterite CZTS, two weaker XRD peaks at 32.28° and 46.38° that belong to anilite Cu_7S_4 (JCPDS 22-0250) are also observed along with the peaks of kesterite CZTS in CZTS_Tu. Since sulphides such as ZnS and Cu_2SnS_3 have similar XRD patterns with CZTS because of their similarity in crystal structure, therefore, it is necessary to employ other techniques such as Raman spectroscopy to distinguish these sulphides impurities in the material.

The Raman spectrum of CZTS_Tu (Fig.1(b)) shows that besides

the characteristic scattering peaks of kesterite CZTS at 287 cm^{-1}, 336 cm^{-1} and 372 cm^{-1}, two peaks at 305 and 359 cm^{-1} which belong to the Raman scattering of cubic Cu_2SnS_3 are also found.[13] Thiourea is commonly used as an organic sulphur precursor for synthesis of sulphides nanocrystals, including CZTS. Liu *et al* reported the successful synthesis of wurtzite CZTS using Tu based hydrothermal method which contained significant amount of organic solvent ethylenediamine (water/ethylenediamine = 9:1).[14] The failure of obtaining compositional-pure CZTS in our case may be due to the difference in the precursor solutions used in the hydrothermal reaction.

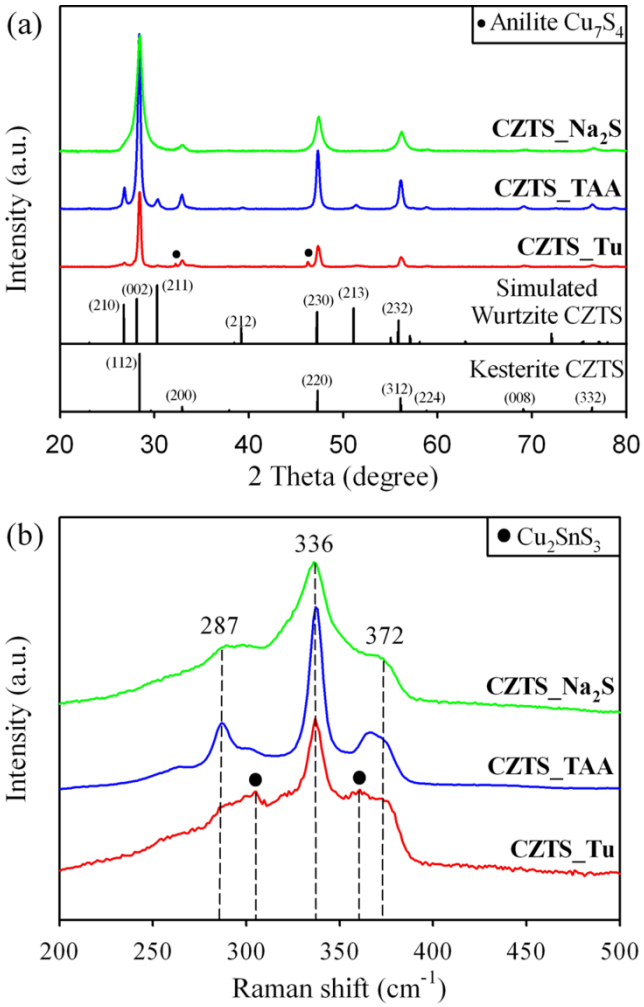

Fig. 1 (a) XRD patterns and (b) Raman spectra of the samples synthesised using different sulphur sources.

Phase-pure CZTS with kesterite structure is obtained using Na_2S as the sulphur precursor in the hydrothermal reaction. As illustrated in Fig. 1(a), all the XRD diffraction patterns of as-synthesised CZTS_Na_2S at 28.46°, 32.94°, 47.30°, 56.10°, 58.88°, 69.10°, 76.38° can be assigned to the corresponding (112), (200), (220), (312), (224), (008), and (332) crystal planes of kesterite CZTS (JCPDS 01-75-4122).[4] The Raman spectrum of CZTS_Na_2S shown in Fig. 1(b) suggests that the strong Raman peaks at 336 cm^{-1} with two shoulder peaks at 288 cm^{-1} and 372 cm^{-1} can be well ascribed to the scattering of kesterite CZTS.[13] The characteristic Raman peaks corresponding to typical sulphides impurities which are normally found in a hydrothermal reaction such as $Cu_{2-x}S$ (475 cm^{-1}), SnS_2 (315 cm^{-1}), ZnS (278 and 351 cm^{-1}), Cu_2SnS_3 (297 and 337 cm^{-1}), and Cu_3SnS_4 (318 cm^{-1}) are not observed in the spectrum. [13, 15] This suggests the high purity of the as-synthesised CZTS_Na_2S material. It is worthy to mention that Camara *et al.* also reported hydrothermal synthesis of CZTS nanoparticles using Na_2S as sulphur source. However, they failed to obtain phase-pure CZTS material. The reason could be due to the different chemical compositions used in the precursor solution. The materials of ethylene glycol and Sn^{2+} were used as the complexing agent and tin source respectively in their hydrothermal system instead of thioglycolic acid and Sn^{4+} in this work.[16] In contrast, the CZTS made from TAA as the sulphur precursor (CZTS_TAA) shows a very different XRD pattern. Besides the four XRD diffraction peaks of kesterite CZTS mentioned above, the peaks at 26.72°, 30.24°, 39.18°, and 51.10° are also observed. These peaks match the diffraction patterns of (210), (211), (212), and (213) planes of wurtzite CZTS instead (details of crystal structure and simulated XRD pattern of wurtzite CZTS are depicted in Table S1 and Fig S1 in the Supporting Information). Similar XRD peaks of wurtzite CZTS but with much weaker intensity are also found with CZTS_Tu. It is worth to note that, similar to kesterite CZTS, wurtzite CZTS also has X-ray diffraction peaks at around 28.40°, 47.30°, and 56.10°.[17] Therefore these three peaks can be ascribed to either the (112), (220), and (312) planes of kesterite CZTS or (002), (230), and (232) planes of wurtzite CZTS. Nevertheless, the weak diffraction peak at around 33°, which is unique to the (200) plane for kesterite CZTS, proves the existence of kesterite CZTS in CZTS_TAA and CZTS_Tu (Fig. 1(a)). It indicates that the synthesised CZTS_TAA and CZTS_Tu materials contain the crystal structure of both kesterite phase and wurtzite phase.[18] In order to determine the abundance of each crystal phase, the XRD patterns are analysed by Rietveld based refinement.[19] The results indicate that wurtzite phases accounts for 25.4% of the material while the rest is dominated by kesterite phase (Fig. S2).

Zou *et al* has reported that the relative reaction rate between Zn^{2+} and sulphur precursor determines the crystal structure of the synthesized CZTS. Fast reaction between Zn^{2+} and sulfur precursors favours the formation of wurtzite CZTS while a slow reaction between them may lead to kesterite phase.[20] The fact that the content of wurtzite in synthesized material following the order of CZTS_TAA > CZTS_Tu > CZTS_Na_2S suggests the relative reaction rate of Zn^{2+} with the sulphide precursor is TAA > Tu > S^{2-}. However, the reactivity between Zn^{2+} and TAA might not be rapid enough to form pure wurtzite crystal structure and the hydrothermal reaction was dominated by the slow reaction step, leading to the formation of both crystal phases. Similar phenomenon of formation of mixture of wurtzite and kesterite phases was also reported in a reaction system where metal acetates of copper, zinc and tin reacted with thiourea in oleyamine.[21]

The average crystallites sizes of the synthesized CZTS_Na_2S and CZTS_TAA materials were determined by Scherrer equation,

$$D_p = 0.94\lambda/(\beta_{1/2}\cos\theta)$$

whereby λ is the X-ray source wavelength, $\beta_{1/2}$ is the line

broadening at half the maximum intensity and θ is the Bragg angle. It indicates that the CZTS in CZTS_Na_2S has an average particle size of 13.2 nm (using 2θ = 28.46) while the mean crystallite size of the wurtzite CZTS is around 14.5 nm (using 2θ = 30.33) and the kesterite is 17 nm (using 2θ=32.9) in CZTS_TAA.

As illustrated in Fig. 1(b), the Raman spectrum of CZTS_TAA is very similar to that of CZTS_Na_2S with scattering peaks at around 286, 337, 366, and 372 cm^{-1},[13] indicating that the different atom arrangement in kesterite and wurtzite crystal structure does not influence their Raman vibration. Other characteristic peaks of impurities are not observed, excluding the formation of secondary phases in the synthesized CZTS_Na_2S and CZTS_TAA.

The chemical compositions of the as-synthesised CZTS nanoparticles investigated by EDS are shown in Table 1. As can be seen, the atomic ratio of Cu/Zn/Sn/S in CZTS_Na_2S and CZTS_TAA is very close to the stoichiometric ratio of 2:1:1:4 of Cu_2ZnSnS_4 compound with Cu/Zn/Sn/S = 1.93/1.00/1.00/3.96 for CZTS_Na_2S and 2.05/1.02/1.00/4.14 for CZTS_TAA respectively. In contrast, it is found the atomic ratio of the synthesized CZTS_Tu material deviates from the stoichiometry of CZTS compound seriously. CZTS_Tu contains much higher content of copper and less zinc with the ratio of [Cu]/ ([Zn]+[Sn]) = 1/0.82 and [Zn]/[Sn] = 1/1.52. This is due to the existence of Cu_2SnS_3 impurity in the hydrothermal products as confirmed by the Raman spectrum discussed before.

Table 1: Elemental analysis of CZTS material synthesised using different sulphur sources

Atomic ratio	CZTS_Na_2S	CZTS_TAA	CZTS_Tu
Cu/Zn/Sn/S	1.92/1.01/1.00/3.96	2.04/1.02/1.00/4.13	3.09/1.0/1.51/4.77
[Cu]/([Zn+Sn])	1/1.05	1/1.01	1/0.82
[Zn]/[Sn]	1/0.99	1/0.99	1/1.52

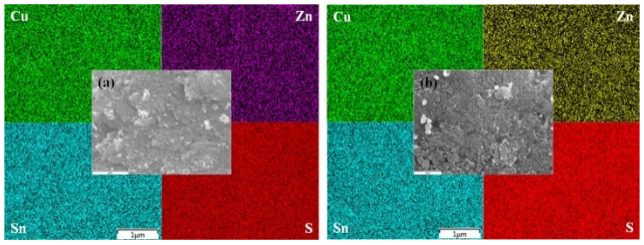

Fig. 2 EDS elemental mapping of (a) CZTS_Na_2S and (b) CZTS_TAA

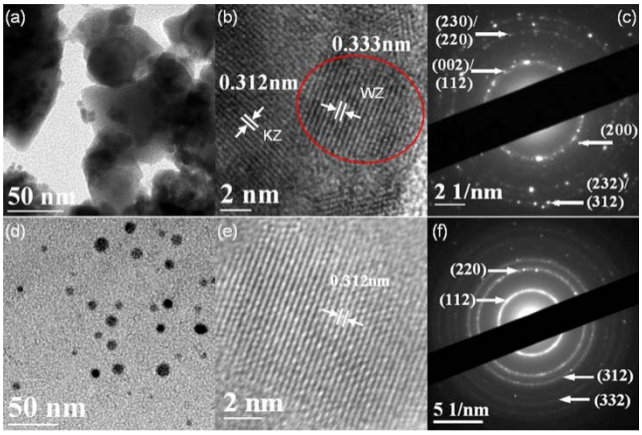

Fig. 3 TEM, HRTEM images and SAED patterns of CZTS_TAA (a, b, c) and CZTS_Na_2S (d, e, f) nanoparticle.

The elemental mapping of CZTS_Na_2S and CZTS_TAA are employed to investigate the homogeneity in terms of material composition. As shown in Fig. 2, the uniform colour of all four elements in the EDS mapping of CZTS_Na_2S and CZTS_TAA suggests that the distributions of Cu, Zn, Sn and S element in both samples are uniform without noticeable compositional variation in the selected area. 10 different areas were selected for EDS mapping and they all showed very similar results. This further confirms the compositional purity of the synthesized material, which is in good agreement with the above XRD and Raman results.

The TEM and HRTEM images of the synthesized CZTS_TAA are shown in Fig. 3 (a, b). It is found that the size distribution of crystallites of CZTS_TAA (Fig. 3(a)) is not uniform. Besides large nanoparticles with size around 50 to 100 nm, smaller nanocrystals with sizes ranging from 8 to 10 nm are also observed. The measurement of the interplanar spacings, *d*, of the crystals shows that *d* = 0.312 nm which is ascribed to the (112) planes of kesterite CZTS. Meanwhile the larger interplanar spacing *d* = 0.33 nm, which is due to the (210) planes of wurtzite CZTS, is also found (Fig. 3(b)). The coexistence of kesterite and wurtzite phases in CZTS-TAA is also confirmed by the selected area diffraction pattern of the material as illustrated in Fig. 3(c). Both (002), (230) and (232) planes of wurtzite CZTS and (112), (200), (220) and (312) planes of kesterite CZTS are found in the SAED pattern, confirming the co-existence of both crystal structures in the material. These results are consistent with the above XRD results.

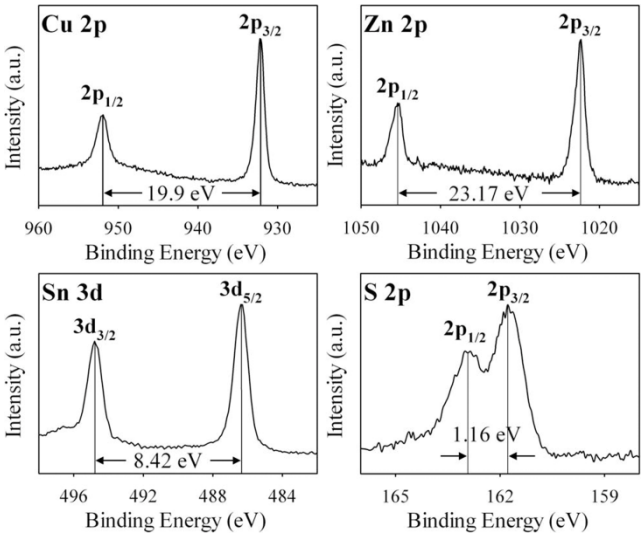

Fig. 4 XPS spectra of CZTS_Na_2S nanocrystals.

In contrast, the crystallites in CZTS_Na_2S (Fig. 3d) are monodisperse nanospheres with size of 10 ± 3 nm, in good agreement with the crystallite size estimated by Scherrer formula. The corresponding HRTEM images (Fig. 3e) confirm the good crystallinity of the synthesised CZTS nanoparticles. The interplanar spacing, d = 3.12 Å in lattice fringe of CZTS_Na_2S which can be ascribed to the (112) plane of kesterite phase CZTS is found. This result indicates that kesterite CZTS grew along the [112] direction in CZTS_Na_2S in the hydrothermal reaction. The diffraction spots in the SAED pattern shown in Fig. 3f can all be well indexed to the corresponding planes of kesterite CZTS.

The valence states of all four elements in the as-synthesised nanoparticles were investigated by XPS. It is worth to note that the measured XPS spectra of both CZTS_Na_2S and CZTS_TAA are found to be same in terms of bonding energy and peak splitting for all four elements. Hence only the XPS spectrum of the four constituent elements: Cu 2p, Zn 2p, Sn 3d and S 2p of CZTS_Na_2S are shown (Fig. 4). As can be seen, the spectrum of Cu 2p shows two peaks appearing at 932.14 and 951.99 eV respectively with a splitting of 19.85 eV, which is in good agreement with the standard separation (19.9 eV) of Cu(I). The peaks at 1022.29 and 1045.46 eV with a split orbit of 23.17 eV can be assigned to Zn(II). The peaks of Sn 3d show binding energies at 486.35 and 494.77 eV respectively, consisting with the value of Sn(IV). The S 2p peaks are located at 161.76 and 162.92 eV, which are in good agreement with the binding energy of sulphur in sulphide state of CZTS. These results are in agreement with the reported values of the binding state of the elements of CZTS,[11] further confirming the phase-purity of the synthesized material.

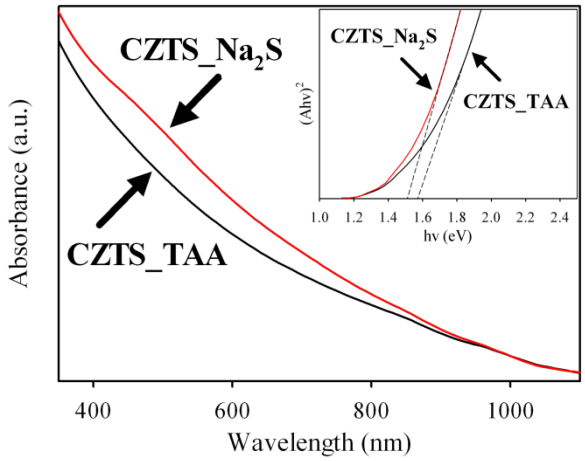

Fig. 5 UV-vis absorption spectra of the as-synthesised CZTS_TAA and CZTS_Na_2S nanoparticles and the inset image shows the $(Ahv)^2$ *vs.* *hv* for the samples.

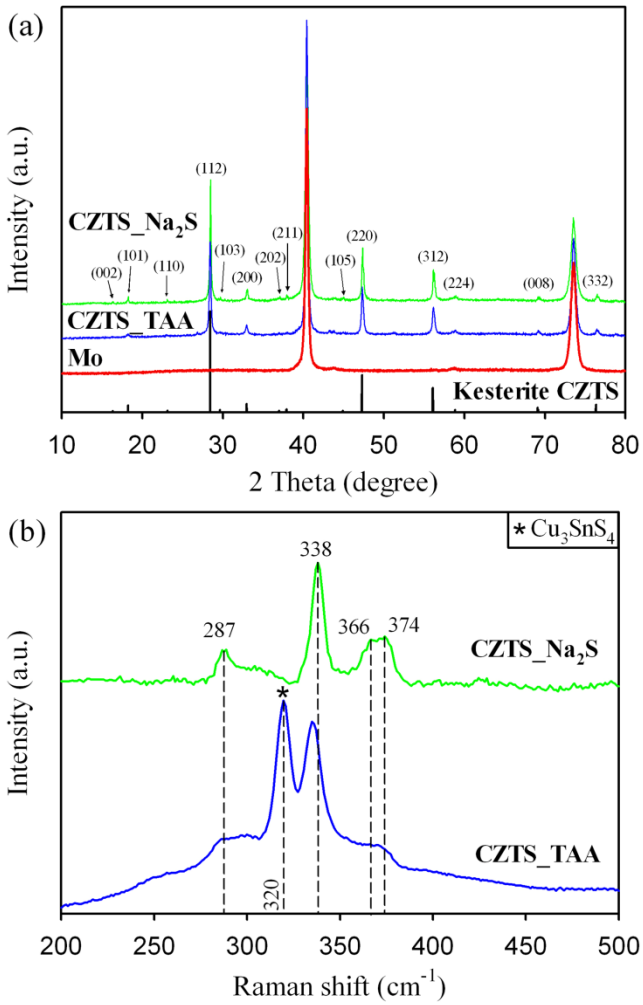

Fig. 6 (a) XRD pattern and (b) Raman spectra of CZTS thin films annealed at 550 °C for 30 mins.

As a promising light absorbing material, strong light absorption over broader range of solar spectrum is desired. The UV-visible absorption spectra of the synthesized CZTS_Na_2S and CZTS_TAA are shown in Fig. 5. Apparently, the light absorption of the both materials extends over 1000 nm, indicating their

broad light absorption characteristics. The band gap is determined by extrapolating the linear part of the plot (inset of Fig. 5) of $(Ahv)^2$ *vs* hv where A = absorbance, h = Planck's constant, and v = frequency of both materials, to zero. The result reveals that the band gap, E_g, for CZTS_Na_2S is 1.51 eV, which is in good agreement with the reported theoretical calculation of kesterite CZTS (E_g = 1.5 eV).[22] In contrast, the band gap of CZTS_TAA is a bit larger with E_g = 1.58 eV, which is attributed to the larger band gap of wurtzite phase in the material due to its lower symmetry in crystal structure.[8] It is worth to note that the weak light absorption of both films beyond 800 nm in the UV-visible spectrum could be due to the scattering effect of the CZTS nanoparticle in ethanol. However, such absorption broadening does not influence the accuracy of the determination of the bandgap because the linear part of $(Ahv)^2$ falls in the wavelength range less than 720 nm.

Deposition of CZTS thin films

CZTS thin films deposited on a Mo/SLG substrate were fabricated to evaluate the photoresponse of the synthesized CZTS materials. Since it has been reported that thermal treatment is beneficial for the performance of solar cells, the films were annealed at different temperatures before assessing their photoactivity under illumination. Both XRD and Raman spectroscopy were employed to scrutinize any change of crystal structure and material composition of the annealed film.

Fig. 6 shows the XRD patterns (a) and corresponding Raman spectra (b) of the annealed CZTS_Na_2S and CZTS_TAA thin films at 550°C for 30 min. Obviously, the crystallinity of the annealed films is improved compared to the film without annealing. More importantly, only kesterite phase CZTS are found in the XRD of both CZTS_Na_2S and CZTS_TAA (Fig. 6(a)). No trace of wurtzite phase CZTS in CZTS_TAA is found, suggesting that the thermal treatment has resulted in the phase transformation from wurtzite CZTS to kesterite phase. Similar phenomenon was also reported by Jiang *et al*.[17] The Raman spectrum of the annealed CZTS_Na_2S thin films at 550 °C confirms that the thermal treatment does not induce any decomposition reaction since no peak corresponding to impurities is observed. However, one strong peak at 320 cm^{-1} appears in the Raman spectrum of the annealed CZTS_TAA film apart from the characteristic CZTS peaks (Fig. 6b). This peak is ascribed to the Raman scattering of Cu_3SnS_4 which was not detected by XRD because of the similarity in its crystal structure with CZTS.[23] It suggests that wurtzite CZTS may partly decompose during thermal treatment.

The above results show that Na_2S is the best sulphur source to produce high purity kesterite CZTS compound which is very stable under high temperature annealing. Thus, the following work is focus on CZTS_Na_2S films.

Fig. 7 (a) shows the cross sectional SEM images and the corresponding EDS elemental mapping of the CZTS_Na_2S thin films annealed at 550 °C. Apparently, the film is densely packed and uniform with a thickness around 1.7 µm. The elemental mapping Cu, Zn, and Sn of the film (at bottom of Fig. 7a) confirms the homogenous distributions of these elements in the film without noticeable compositional variation. It is also noticed that there is no observable change in grain size in the film after annealing at 550 °C.

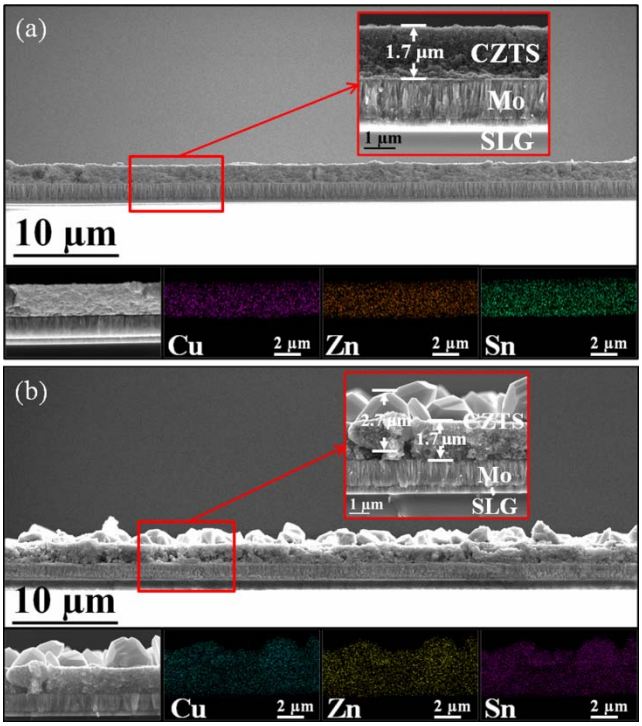

Fig. 7 Cross sectional SEM images and EDS elemental mapping of CZTS_Na2S thin film annealed at (a) 550 °C for 30 mins and (b) 600 °C for 3 h.

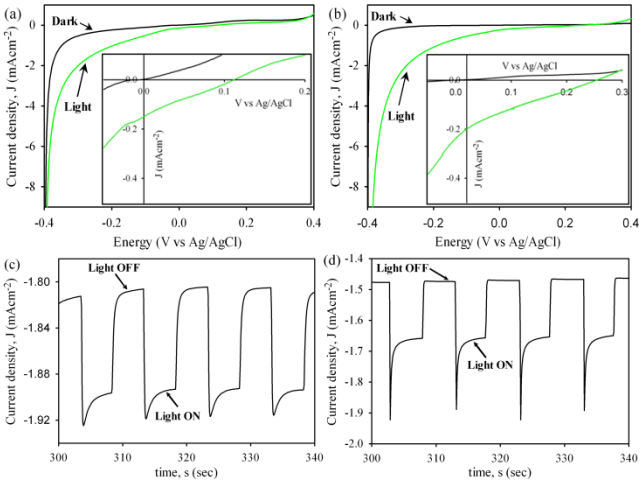

Fig. 8 *J-V* plots and voltammogram of the CZTS_Na_2S thin film annealed at (a, c) 550 °C and (b, d) 600 °C, with the insets of (a) and (b) displaying the enlarged plot.

Nevertheless, when the annealing temperature was increased to 600°C and the duration was increased to 3 h, large grains of CZTS crystals with size over 2.5 µm are found on the surface of the film (Fig. 7b)). Some grains even grow through the whole film (Fig. 7b, inset). The average thickness of the film remained at around 1.7 µm. Compare to the film annealed at 550°C, the uniformity of the film annealed at 600 °C is reduced because of the formation of the large grains. It has been reported that the carbon-containing solvent used in the colloid preparation for thin film coating (e.g. terpineol and triton X-100 in our case) is harmful for the formation of large crystals.[24] This could explain that the major part of the film still consists of small grains. The elemental mapping of CZTS film annealed at 600 °C (at bottom

of Fig. 7(b)) confirms the homogenous distribution of Cu, Zn, and Sn element in the film with atomic ratios close to the stoichiometry of 2:1:1 in CZTS. No Sn loss was observed throughout the film even though the annealing temperature was well above 500 °C.[25, 26]

Photoactivity investigation of CZTS thin films

Fig. 8(a) and (b) show a current-voltage (*J-V*) curve of the annealed CZTS nanocrystals thin film at different temperature under dark and under illumination provided by a light emitting diode (LED, 532 nm). The photocurrent of the CZTS films under illumination was measured after 15 mins of light soaking, which may increase the transient photocurrent of the absorber films compared to the film without light soaking. The *J-V* plot of the cell under dark goes through zero while a cathodic photocurrent is observed for the film annealed at 550 °C and 600 °C under illumination. The cathodic photocurrent increases gradually with the increase of the negative bias, which indicates that the p-type conductive nature of the synthesized CZTS material.[27] It is also noticed that both the J_{sc} and V_{oc} of the film annealed at 600 °C are larger than the film thermally treated at 550 °C, confirming the benefit of large grains in the film.

The stability of the photocurrent of CZTS thin films is evaluated at a constant potential of -300 mV (*vs.* Al/AgCl reference) by chopping the light on/off with 5 seconds intervals (Fig. 8(c) and (d)). The CZTS film annealed at 550 °C (Fig. 8(c)) shows a photocurrent density of 0.087 mA/cm^2 that slightly increases over time under illumination. In contrast, a higher photocurrent density was generated by film annealed at 600 °C (0.2 mA/cm^2) and the photocurrent was very stable under the same illumination condition (Fig. 8(d)). The higher photocurrent is attributed to the large grains in the film which should reduce the electron recombination between the generated electron-hole pair owing to reduced grain boundaries. These results indicate that large grain of light absorber in thin film is preferable for application in solar cells in term of enhancing the performance of the device. The initial decay of the transient photocurrent is observed in both films, which could be due to the electron-hole recombination at the surface of the CZTS grains.

Conclusions

High quality quaternary Cu_2ZnSnS_4 (CZTS) nanocrystals have been successfully synthesised using water based one-step hydrothermal route. It has been found that the sulphur precursor used in the hydrothermal system has significantly effect on the phase purity and crystal structure of the synthesized CZTS material. Pure kesterite phase has been obtained when using Na_2S as the sulphur source in the hydrothermal reaction while a mixture of kesterite phase and wurtzite crystal phase CZTS was made when using organic sulphur thioacetamide as the sulphur precursor. Refinement of the XRD result of the material with mixture crystal phases has indicated that the kesterite phase accounted for around 74% with the rest as wurtzite phase. The band gap of the mixture phase material (E_g = 1.58 eV) is slightly larger than that of pure kesterite CZTS (E_g = 151 eV). Thin films using the as-synthesized CZTS_Na_2S nanocrystals were made and were subjected to thermal treatment. Large grains with size around 2.0 μm were found on the surface of the film annealed at 600 °C while there was little change in terms of crystal size in the film annealed at 550 °C. Compared to the film thermally treated at 550 °C, the film annealed at 600 °C also showed higher and more stable photocurrent in photoelectrochemical measurement, which is attributed to the large grains formed in the film, leading to reduced recombination between electron-hole pair in the film.

Acknowledgements

The authors appreciate the technical support for material characterization by Institute of Future Environment, Queensland University of Technology. This work was funded by Australian Research Council (ARC) Future Fellowship (FT120100674), Australia. Yi Zhang acknowledges the financial support from National Natural Science Foundation of China (61274053).

Notes and references

[a] *School of Chemistry, Physics and Mechanical Engineering, Science and Engineering Faculty, Queensland University of Technology, Brisbane, QLD 4001, Australia;. E-mail: hx.wang@qut.edu.au*
[b] *Institute of Photoelectronic Thin Film Devices and Technology, Nankai University, Tianjin 300071, China.*

† Electronic Supplementary Information (ESI) available: Cystal data and structure of simulated wurtzite CZTS and the refinement of the XRD data of CZTS_TAA. See DOI: 10.1039/b000000x/

1. H. Wang, Y. Zhang, X. L. Kou, Y. A. Cai, W. Liu, T. Yu, J. B. Pang, C. J. Li and Y. Sun, *Semicond. Sci. Technol.*, 2010, **25**, 055007.
2. B.-Y. Li, Y. Zhang, H. Wang, B. Wang, L. Wu and Y. Sun, *Progress in Photovoltaics: Research and Applications*, 2013, **21**, 838-848.
3. H. Wang, *Int. J. Photoenergy*, 2011, **2011**, 10.
4. Q. Guo, H. W. Hillhouse and R. Agrawal, *J. Am. Chem. Soc.*, 2009, **131**, 11672-11673.
5. B. Shin, O. Gunawan, Y. Zhu, N. A. Bojarczuk, S. J. Chey and S. Guha, *Progress in Photovoltaics: Research and Applications*, 2013, **21**, 72-76.
6. T. K. Todorov, J. Tang, S. Bag, O. Gunawan, T. Gokmen, Y. Zhu and D. B. Mitzi, *Adv. Energy Mater.*, 2013, **3**, 34-38.
7. S. Y. Chen, X. G. Gong, A. Walsh and S. H. Wei, *Appl. Phys. Lett.*, 2009, **94**.
8. S. Chen, A. Walsh, Y. Luo, J.-H. Yang, X. G. Gong and S.-H. Wei, *Physical Review B*, 2010, **82**, 195203.
9. M. Cao and Y. Shen, *J. Cryst. Growth*, 2011, **318**, 1117-1120.
10. Y.-L. Zhou, W.-H. Zhou, Y.-F. Du, M. Li and S.-X. Wu, *Mater. Lett.*, 2011, **65**, 1535-1537.
11. S. C. Riha, B. A. Parkinson and A. L. Prieto, *J. Am. Chem. Soc.*, 2009, **131**, 12054-12055.
12. M. Wei, Q. Du, D. Wang, W. Liu, G. Jiang and C. Zhu, *Mater. Lett.*, 2012, **79**, 177-179.
13. P. A. Fernandes, P. M. P. Salomé and A. F. da Cunha, *J. Alloys Compd.*, 2011, **509**, 7600-7606.
14. W. C. Liu, B. L. Guo, X. S. Wu, F. M. Zhang, C. L. Mak and K. H. Wong, *J. Mater. Chem. A*, 2013, **1**, 3182-3186.
15. A. J. Cheng, M. Manno, A. Khare, C. Leighton, S. A. Campbell and E. S. Aydil, *J. Vac. Sci. Technol., A*, 2011, **29**, 051203-051211.
16. S. M. Camara, L. Wang and X. Zhang, *Nanot.*, 2013, **24**, 495401.
17. H. Jiang, P. Dai, Z. Feng, W. Fan and J. Zhan, *J. Mater. Chem.*, 2012, **22**, 7502-7506.

18. X. Lu, Z. Zhuang, Q. Peng and Y. Li, *Chem. Commun.*, 2011, **47**, 3141-3143.
19. H. Rietveld, *Acta Crystallogr.*, 1967, **22**, 151-152.
20. Y. Zou, X. Su and J. Jiang, *J. Am. Chem. Soc.*, 2013, **135**, 18377-18384.
21. P. K. Sarswat and M. L. Free, *J. Cryst. Growth*, 2013, **372**, 87-94.
22. C. Persson, *J. Appl. Phys.*, 2010, **107**.
23. P. A. Fernandes, P. M. P. Salomé and A. F. d. Cunha, *J. Phys. D: Appl. Phys.*, 2010, **43**, 215403.
24. H. Zhou, W.-C. Hsu, H.-S. Duan, B. Bob, W. Yang, T.-B. Song, C.-J. Hsu and Y. Yang, *Energy Environ. Sci.*, 2013, **6**, 2822-2838.
25. A. Redinger, D. M. Berg, P. J. Dale and S. Siebentritt, *J. Am. Chem. Soc.*, 2011, **133**, 3320-3323.
26. J. J. Scragg, J. T. Wätjen, M. Edoff, T. Ericson, T. Kubart and C. Platzer-Björkman, *J. Am. Chem. Soc.*, 2012, **134**, 19330-19333.
27. J. J. Scragg, P. J. Dale and L. M. Peter, *Electrochemistry Communications*, 2008, **10**, 639-642.

Table of Contents

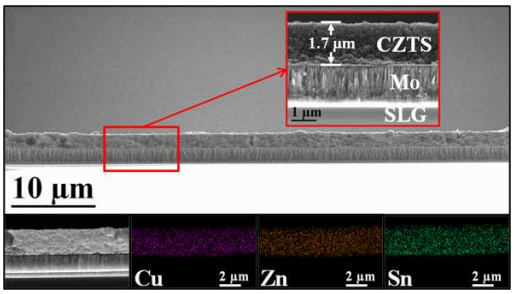

Novelty highlight:

CZTS thin films with uniform thickness and homogeneous composition for generation of stable photocurrent were made using one-step hydrothermal synthesis.